Journal of Power Sources 196 (2011) 3003–3008

Contents lists available at ScienceDirect

Journal of Power Sources

journal homepage: www.elsevier.com/locate/jpowsour

Corrosion of carbon supports at cathode during hydrogen/air replacement at anode studied by visualization of oxygen partial pressures in a PEFC—Start-up/shut-down simulation

Yuta Ishigami[a], Kenji Takada[a], Hiroshi Yano[b], Junji Inukai[b,*], Makoto Uchida[b], Yuzo Nagumo[c], Tsuyoshi Hyakutake[d], Hiroyuki Nishide[d,**], Masahiro Watanabe[b,***]

[a] Interdisciplinary Graduate School of Medicine and Engineering, University of Yamanashi, 4-3 Takeda, Kofu 400-8511, Yamanashi, Japan
[b] Fuel Cell Nanomaterials Center, University of Yamanashi, 6-43 Miyamae-cho, Kofu 400-0021, Yamanashi, Japan
[c] Shimadzu, 3-9-4 Hikaridai, Seika-cho, Kyoto 619-0237, Japan
[d] Department of Applied Chemistry, Waseda University, 3-4-1 Okubo, Shinjuku, Tokyo 169-8555, Japan

ARTICLE INFO

Article history:
Received 22 September 2010
Received in revised form
17 November 2010
Accepted 18 November 2010
Available online 24 November 2010

Keywords:
Polymer electrolyte fuel cell
Degradation
Carbon corrosion
Start-up/shut-down cycles
Visualization of oxygen partial pressure

ABSTRACT

During start-up/shut-down processes of a polymer electrolyte fuel cell, platinum particles are lost from the catalyst layer at the cathode due to corrosion of the carbon supports. We simulated the start-up/shut-down cycle by exchanging gases at the anode between hydrogen and air. During the gas exchange, the distribution of oxygen partial pressures at the anode was visualized by our *real-time*/*space* visualization system, which clearly showed the location of H_2- and O_2-rich areas along the gas-flow channel from the inlet to the outlet. The gas exchange rate was found to be much slower than that predicted from the simple replacement and to be correlated to the proton transfer derived from carbon corrosion of the cathode catalyst layer. By the visualization results, it was found that the shut-down process gives more serious effect than the start-up process. After the degradation, the oxygen partial pressure at the cathode was visualized during the cell operation. Oxygen was consumed mainly in the middle of the MEA because the MEA was degraded mainly near the inlet and outlet of reactant gases in the cell.

1. Introduction

Polymer electrolyte fuel cells (PEFCs) are expected as a clean source of energy, because of their high efficiency and low emission. For higher performances and durability, the degradation problems must be solved. One of the distinct degradation modes is start-up/shut-down cycling of the cell. During the cycles, air and hydrogen coexist in a channel of the anode, generating potential differences in the upper and lower parts of the anode under the presence of air in the cathode [1–16]. At the anode, an oxygen reduction reaction (R1) and a hydrogen oxidation reaction (R2) occur to maintain the electrochemical potential of electrons uniform over the whole anode surface.

$$\text{Anode, } O_2 \text{ region}: \quad O_2 + 4H^+ + 4e^- \rightarrow 2H_2O \tag{R1}$$

$$\text{Anode, } H_2 \text{ region}: \quad 2H_2 \rightarrow 4H^+ + 4e^- \tag{R2}$$

Protons produced in (R2) hardly participate in (R1); a large ohmic resistance exists between O_2 and H_2 regions because of the two-dimensional diffusion of protons from the H_2 region to the O_2 region. Protons in (R1) should, therefore, be supplied through the other shorter paths with lower conduction resistance. It is reported that protons consumed at the anode (R1) are produced by a corrosion of carbon supports (R3) in the cathode catalyst layer, and they are transferred across the thin electrolyte membrane and react with oxygen molecules [1]. As another route for the proton formation, (R4) can also be considered. On the other hand, the main reaction at the cathode is (R5), driven by the counter reaction, (R2), under a sufficient oxygen supply.

$$\text{Cathode, corrosion}: \quad C + 2H_2O \rightarrow CO_2 + 4H^+ + 4e^- \tag{R3}$$

$$\text{Cathode, hydrolysis}: \quad 2H_2O \rightarrow O_2 + 4H^+ + 4e^- \tag{R4}$$

$$\text{Cathode, main reaction}: \quad O_2 + 4H^+ + 4e^- \rightarrow 2H_2O \tag{R5}$$

Nano-sized electrocatalyst particles on the carbon supports are dropped off by the corrosion reaction above, (R3), which eventually causes a distinct decrease in cell performance. This degradation at start-up/shut-down must be avoided.

In situ observations of the distribution of reactants, water, and temperature under operation help to understand the reactions

* Corresponding author. Tel.: +81 55 254 7129; fax: +81 55 254 7129.
** Corresponding author. Tel.: +81 3 3200 2669; fax: +81 3 3209 5522.
*** Corresponding author. Tel.: +81 55 254 7091; fax: +81 55 254 7091.
E-mail addresses: jinukai@yamanashi.ac.jp (J. Inukai), nishide@waseda.jp (H. Nishide), m-watanabe@yamanashi.ac.jp (M. Watanabe).

0378-7753/$ – see front matter © 2010 Elsevier B.V. All rights reserved.
doi:10.1016/j.jpowsour.2010.11.092

proceeding in fuel cells and may lead to optimizations of structures of MEAs, flow fields of separators. They should also be useful in optimize operation modes such as cell temperature, humidification temperature, or the start-up/shut-down procedures mentioned above. The generation or the distribution of liquid water inside the fuel cells has been actively studied and successfully visualized by direct optical observation [17–20], neutron radiography imaging [21–28], X-ray imaging [29–32], and magnetic resonance imaging (MRI) [33–35]. Oxygen partial pressure (p_{O_2}) is also an essential factor, and we have developed a nondestructive, *real-time/space* visualization system for p_{O_2} in operating fuel cells [36,37].

In this paper, distributions of p_{O_2} at the anode were visualized in *real time* and *space* during the start-up/shut-down cycles by our visualization technique. With these results, we will make clear the corrosion behavior at the cathode during the start-up/shut-down processes. We also visualized the distributions of p_{O_2} at the cathode before and after the degradation in an operating PEFC to understand the degradation areas on the MEA.

2. Experimental

2.1. Experimental setup

Fig. 1(a) is a front-view photograph of the visualization cell. Fig. 1(b) shows schematic drawings inside the visualization cell (a transparent endplate, a dye-coated PFA (Perfluoroalkoxy) sheet, a current collector with the gas flow channel, and an MEA). This cell was fabricated by modifying a "JARI Cell (Japan Automobile Research Institute Cell)" with 27 cm^2 of an electrode active area. A stainless-steel endplate used for the conventional JARI cell was replaced by a transparent acrylic endplate. The gas flow field with single serpentine (1429 mm) was machined through a stainless-steel plate with 1 mm thickness and gold-plated. The plate was also used for the current collection. As an oxygen-sensitive dye, porphyrin, [Tetrakis(pentafluorophenyl)porphyrinato]platinum (PtPP), was used for the visualization of p_{O_2}. A toluene solution of PtPP and poly(1-trimethylsilyl-1-propyne), an oxygen permeable matrix for the former, was sprayed, and a uniform film with approximately 2 μm in thickness was formed on the PFA sheet faced to the gas flow channel. Cell performance of the visualization cell used was nearly identical to that of the JARI cell without a dye coating.

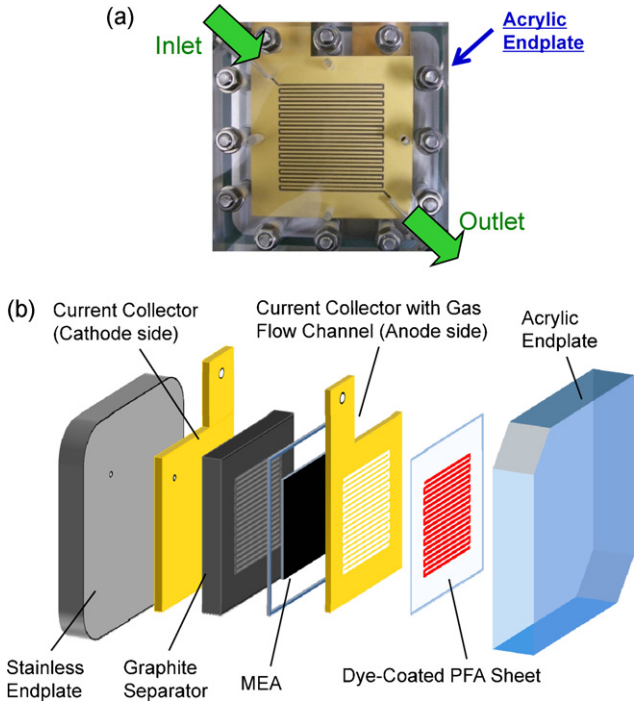

Fig. 1. Visualization cell. (a) Photograph taken from the front. (b) Schematic drawings of the cell with a transparent endplate, a dye-coated sheet, a current collector with the gas flow channel, and an MEA.

For the visualization, a 407-nm excitation light from a diode laser was diffused, spread and distributed uniformly onto the visualization cell. The emission from the dye film through the acrylic plate was filtered (>600 nm), and images of the emission from the dye film were captured with a CCD camera (500 × 500 pixels, 1 pixel = 100 × 100 μm) in a dark room.

2.2. Real-time visualization of p_{O_2} at the anode during gas exchange

To obtain the calibration curves for p_{O_2} at all segments in the channel, Stern–Volmer plots were first acquired by introducing mixed gases containing oxygen in nitrogen from 0 to 25% to both anode and cathode channels at 50 ml min^{-1} under ambient pressure in the same procedure as reported in previous papers [36]. The gas-exchange cycling experiments were performed as in the following manner. First, the anode gas channel was filled with air. Then every 30 s, the anode gas was exchanged from air to hydrogen (start-up simulation), and from hydrogen to air (shut-down simulation). To the cathode, air was continuously supplied. The gas-flow rates both in the anode and cathode gas-flow channels under ambient pressure were the same, 100 ml min^{-1}, equivalent to an linear flow rate of 167 cm s^{-1}. The cell temperature was set at 80 °C, and gases were humidified at 40% RH. The gas-exchange cycling was carried out up to 500 cycles. After the first cycle and then after 100, 300, and 500 cycles, p_{O_2} changing during the gas exchange process at the anode was visualized with a CCD camera by capturing images continuously. The time and space resolutions were 200 ms and 100 μm, respectively. Captured images were converted to p_{O_2} images using the Stern–Volmer plots acquired in advance. *I–V* curves were also acquired in the conventional manner.

2.3. Visualization of p_{O_2} at the cathode before and after the degradation

Visualization of p_{O_2} at the cathode in a running cell was carried out before and after the cathode degradation (500 cycles) caused by the gas exchange at the anode. The cell temperature was set at 80 °C, and hydrogen and air at 60% RH were supplied at 300 ml min^{-1} to the anode and the cathode gas-flow channels, respectively. The oxygen consumption was set at 0, 20 and 40%. We captured and averaged 32 images.

2.4. MEA observation after degradation with a scanning transmission electron microscope

After the visualization experiments, the MEA was taken out from the cell. Samples 90 nm in thickness were prepared by using a microtome (LEICA ULTRACUT UCT). The cross-sections of the catalyst layers at the anode were observed with a scanning transmission electron microscope (STEM) (Hitachi HD-2300C, acceleration voltage = 200 kV).

3. Results and discussion

3.1. I–V curves during the simulated start-up and shut-down cycles

I–V curves before the gas-exchange cycling and after 100, 300, and 500 gas-exchange cycles are shown in Fig. 2. On a fresh MEA

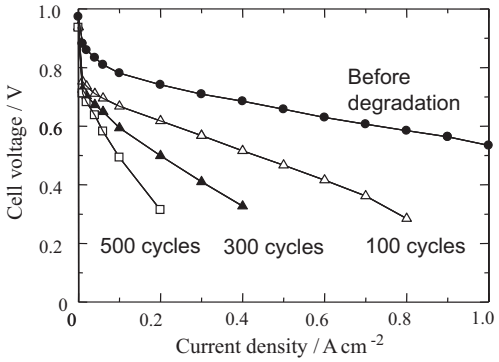

Fig. 2. *I–V* curves during the gas-exchange cycling. Anode gas was exchanged from air to H_2 (simulating start-up process) and from H_2 to air (simulating shut-down process) at an interval of 30 s.

before the cycling test, the steady *I–V* curve was obtained by using the visualization cell. The *I–V* curve was almost the same as that obtained with a conventional JARI cell. At 0.8 A cm^{-2}, for example, the voltage was 0.59 V before degradation. Only after 100 cycles, the cell voltage drastically dropped to 0.28 V, and further cycling lowered the performance continuously. Therefore, this gas-exchange cycling test, simulating the start-up/shut-down process, was able to be used to study degradation behaviors in a PEFC in an accelerated mode.

3.2. Real-time visualization of p_{O_2} at the anode during the gas-exchange cycles

Fig. 3 shows the p_{O_2} visualization at the anode when the anode gas was exchanged from hydrogen to air. Video 1 in supplementary data shows the *real-time* p_{O_2} images at the anode before and after degradation. The upper images in Fig. 3 were obtained before degradation and the lower images after 500 cycles of gas exchange. First, the anode gas flow channel was filled with hydrogen, where $p_{O_2} = 0$ kPa. Air was then supplied at 100 ml min^{-1}. As shown in the figure, p_{O_2} increased with increasing time from the inlet along the gas flow channel down to the outlet. Before the completion of the gas exchange, a hydrogen-rich area (blue area) and an oxygen-rich area (red area) appear simultaneously on the MEA for a certain period. As a function of exchanging time, the locations of the O_2- and H_2-rich areas in the anode are clearly shown. It is also notable that the complete exchange of the gases required obviously a longer time than that expected from the simple gas replacement as will be discussed below.

Hereinafter, the time required for the gas replacement is defined as a "replacement time" for convenience. We can now understand the carbon corrosion process [1] intuitively by the present visualization system and more quantitatively using the replacement time. At the anode, the electrochemical potential becomes higher in the O_2-rich area (giving rise to (R1)) due to the presence of remaining hydrogen (causing the overwhelming major and fast (R2)). From the Nernst equation, a higher electrochemical potential could be estimated to become a several hundreds of mV vs. the reversible hydrogen electrode for the O_2-rich area, if enough protons were supplied in (R1). This higher potential brings about increase of the potential in the area of the opposite-side cathode, resulting in the corrosion of carbon supports (R3) as a counter reaction of (R1) at the anode. Thus, in the case of the gas exchange from hydrogen to air, the degradation by carbon corrosion is predicted to proceed mainly in the upper part of the PEFC because of the longest exposure to O_2-rich atmosphere for the replacement time in the cell. The volume in the anode gas-flow channel is 1.43 ml. The gas flow rate (100 ml min^{-1}) being considered, the time required for the simple replacement of hydrogen in the channel with air is calculated to be only 0.86 s. However, from the result of the p_{O_2} visualization, the gas exchange took approximately 6 s. Such a big difference in the replacement time is first discovered with the present visualization technique. The co-existence of H_2- and O_2-rich areas in the anode presumably makes the serious corrosion at the cathode. This long exchange time may be resulted from the combination of the following three replacement processes, abbreviated as RP. The time delay relating to the replacement of hydrogen previously existing in the channel could be ignored because it is regarded as a simple process of push-out.

(RP-1) Replacement of hydrogen with air by diffusion inside of the cell including the GDL.
(RP-2) Reaction between O_2 and H adsorbed on the anode catalyst surface (R6)
(RP-3) Consumption of O_2 (R1) by protons transferred from the cathode after the carbon-support degradation by the corrosion (R3)

$$\text{Anode}: \quad 4H_{ads} + O_2 \rightarrow 2H_2O \quad \text{or} \quad 2H_2 + 2O_{ads} \rightarrow 2H_2O \qquad \text{(R6)}$$

In (R6), a trace of H_2O_2 could be produced as a byproduct. For (RP-1), the space volume inside the GDL is calculated to be 0.50 ml.

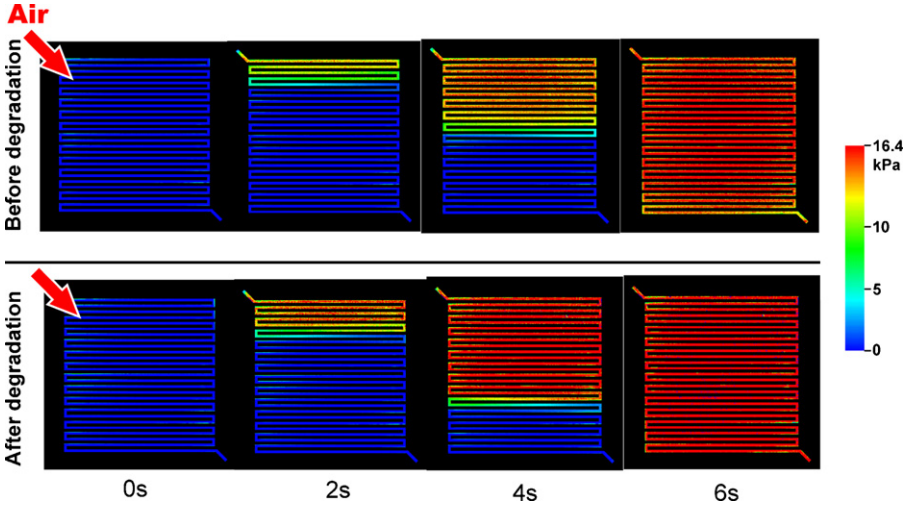

Fig. 3. Visualization of p_{O_2} at the anode during the gas exchange from H_2 to air before and after the deterioration of the cell performances by 500 cycles of the gas exchange.

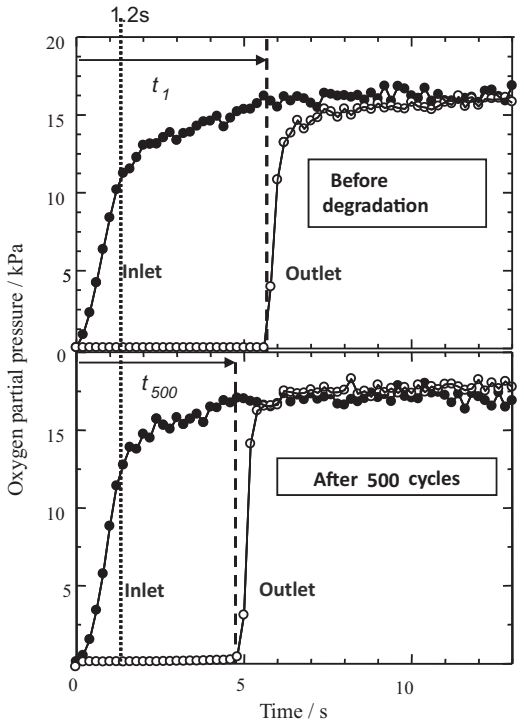

Fig. 4. p_{O_2} at the inlet and the outlet of the flow channel during the gas exchange from H_2 to air, analyzed from the data in Fig. 3.

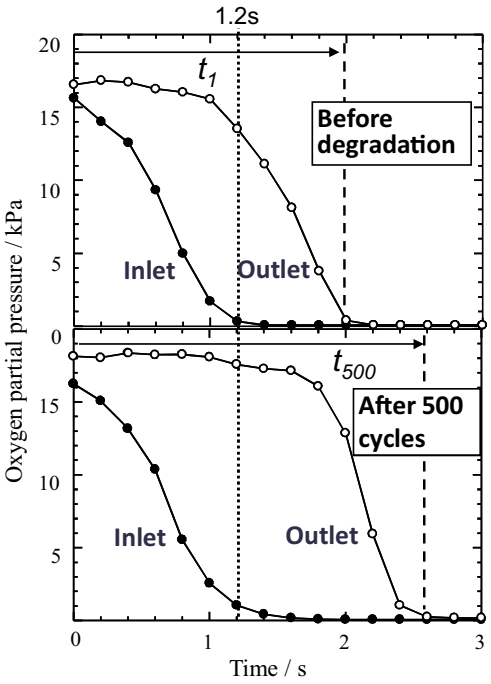

Fig. 6. p_{O_2} at the inlet and the outlet of the flow channel during the gas exchange from air to H_2, analyzed from the data in Fig. 5.

With the volume of the gas flow channel, 1.43 ml, the volume through which gases run in the cell is summed up as 1.93 ml. In the simple, "physical" gas-replacement process, the replacement time is thus calculated as 1.2 s (longer by 0.3 s considering the space volume of the GDL); this value is still much smaller than the measured time, 6 s. The number of hydrogen atoms adsorbed on the platinum surface was calculated, and the oxygen used for (RP-2) was estimated to be only 10% of the oxygen flow. This will make the replacement time longer only by 0.2 s. Therefore, (RP-1) (0.3 s) and (RP-2) (0.2 s) could not be the main reasons for the long gas-exchange time; (RP-3) should be the reason. Although the direct effects of (RP-1) and (RP-2) are small, the prolonged replacement time results in more carbon corrosion at the cathode (R3), eventually causing (RP-3). For more detailed discussion, the changes of p_{O_2} at the inlet and outlet portions in the anode are shown in Fig. 4, plotted as a function of time after the switching from hydrogen to air based on the data shown in Fig. 3. In the cell before the degradation by gas-exchange cycles, p_{O_2} at the inlet part increases steeply up to approximately 75% to that in pure air for 1.2 s (replacement time for "physical" gas exchange); p_{O_2} keeps increased gradually, and approximately 6 s is needed for the compete replacement with air. In Fig. 4, it can be seen that around 5 s, p_{O_2} at the outlet part increases steeply and shortly reaches to that of pure air without the slow increase process found at the inlet part. For more quantitative analysis, t_n is defined as the time between the raisings of p_{O_2} at the inlet and the outlet for the index for the gas replacement. The t_{500} was found to be shorter than t_1 by approximately 1 s. We believe that this time difference, Δt, is related to the degradation of the cathode catalyst layer, which will be discussed later.

Fig. 5 shows the p_{O_2} visualization at the anode when the anode gas was exchanged from air to hydrogen as a stating-up simulation. Fig. 6 shows p_{O_2} at the inlet and the outlet during the gas exchange. Video 2 in supplementary data shows the *real-time* p_{O_2} images at

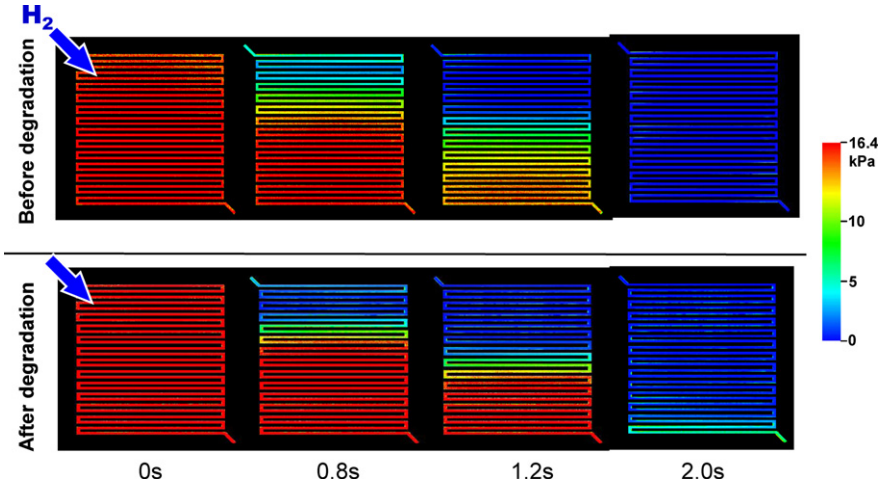

Fig. 5. Visualization of p_{O_2} at the anode during the gas exchange from air to H_2 before and after the deterioration of the cell performances by 500 cycles of the gas exchange.

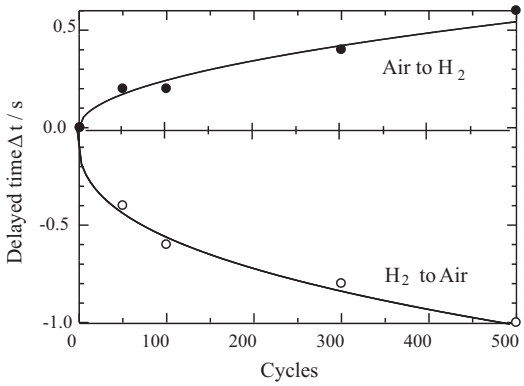

Fig. 7. Δt vs. the number of gas-exchange cycles for the gas exchange from air to H_2 (upper half) and H_2 to air (lower half).

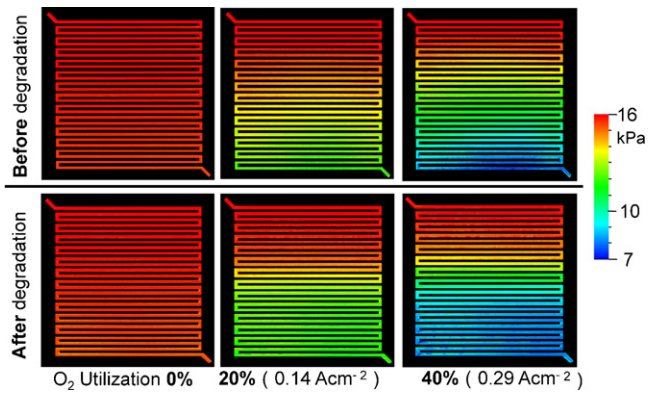

Fig. 8. Changes of p_{O_2} at the cathode during the cell operation before and after the deterioration of the cell performances.

the anode before and after degradation. Before degradation, the air in the channel was completely exchanged by hydrogen within 2 s as shown in Figs. 5 and 6, a time much shorter than that of the reverse gas replacement for the shutting-down simulation, i.e., by approximately 4 s. Therefore, the cathode corrosion could be prevented rather easily at the starting-up process. The reason for the higher gas-exchange rate with hydrogen might be explained by a high reaction rate of (R2), i.e., an electrochemical potential of the portion accessed by hydrogen instantaneously establishes the reversible potential (approximately 0 mV) for (R2), so that O_2 or adsorbed oxygen should be reduced by (R1). Protons formed in (R2) are consumed in (R1), and O_2 in air is consumed in (R6) in addition to (R1) and with protons formed in (R3) in the down-flow area. After 500 gas-exchange cycles, the exchanging time became longer, contrary to the result of the gas exchange from hydrogen to air, which can be attributed to delayed O_2 consumption via (R2) or (R6).

The corrosion behavior was investigated more quantitatively at both gas-exchange processes by plotting the relationship between p_{O_2} and the delayed time Δt ($=t_n - t_1$) in Fig. 7 for the various cycle number (n) of gas-exchange processes, compared with those before the degradation. It is clear that the replacement time from hydrogen to air decreased ($0 > \Delta t$) steeply and that from air to hydrogen increased ($0 < \Delta t$) with increasing the cycling number, n. We believe that these time differences are related to the degradation of the cathode catalyst layer. As the number of gas-exchange cycles increases, the rate of the degradation itself may be lowered as reported in literatures [2,10]. If it happens, protons transferred from the cathode to the anode should be decreased after the cycles, resulting in the decrease in the amount of oxygen molecules reacting with protons. This should lead to the faster replacement of hydrogen by air in the gas channel, as seen in Fig. 7. On the other hand, the replacement time from air to hydrogen became obviously longer than the non-degraded cell. As discussed above, O_2 consumption in air via (R1) and (R2) in the down-flow area in the cathode should be lowered at the degraded cell by the cathode corrosion.

3.3. Visualization of p_{O_2} at the degraded cathode under the cell operation

Before degradation and after 500 gas-exchange cycles, p_{O_2} at the cathode was visualized under the operating conditions. The upper three images in Fig. 8 are those for different oxygen utilizations ($U_{O_2} = 0, 20,$ and 40%) before the degradation test, and the lower three are those after degradation. As the oxygen utilization was increased, p_{O_2} became more decreased along the flow channel both before and after the degradation tests. The p_{O_2} values at the cathodes are plotted in Fig. 9 along the flow channel (1429 mm in length) from the inlet to the outlet at $U_{O_2} = 40\%$ before and after the degradation. Before degradation (line in blue), oxygen was uniformly consumed along the flow channel, whereas after degradation (line in red), oxygen was mainly consumed at the middle of the MEA (at approximately 500–900 mm) showing a steep change in slope. Therefore, the degradation was found to occur distinctively at the upper and lower parts of the MEA [6]. These results show that we can clearly detect the corrosion levels or positions depending on the cycling number or the mode of the start-up/shut-down by this nondestructive analysis.

3.4. STEM images at the cathode catalyst layer

Fig. 10 shows STEM images near the inlet, the center, and the outlet at the cathode catalyst layer after 500 cycles of the hydrogen/air replacement. In the images obtained near the inlet, holes (0.5–1 μm in diameter) shown by circles are apparent with no carbon support, indicating a drastic corrosion of carbon. At the center, no such holes are seen, showing that the catalyst layer is much less degraded. Near the outlet, holes again appear. In Fig. 9, it was shown that oxygen is mostly consumed in the center of the MEA, suggesting that the degradation occurred mainly near the inlet and the outlet. The STEM images clearly show the corrosion near the inlet and the outlet. This distinct degradation of the catalyst layer quickly lowered the cell performance as shown in Fig. 2.

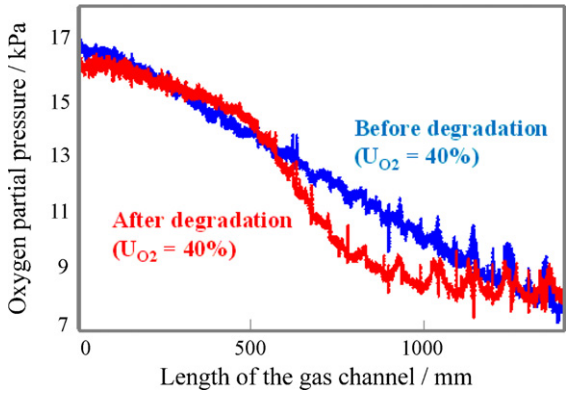

Fig. 9. Changes of p_{O_2} along the flow channel from the inlet to the outlet before and after the degradation. Oxygen utilization = 40%. Blue and red lines are for results obtained before and after degradation, respectively. Air flow rate = 300 ml min^{-1}.

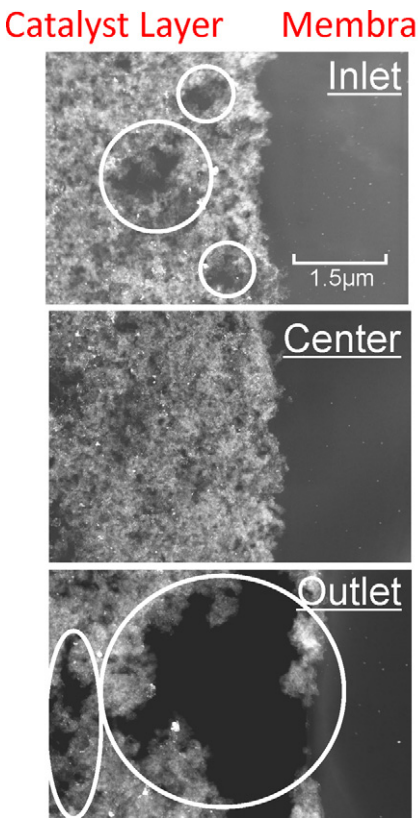

Fig. 10. STEM images near the inlet, the center, and the outlet of the MEA at the cathode after the degradation.

4. Conclusions

By visualizing p_{O_2} at the anode and the cathode, the degradation of the cathode, accompanied with hydrogen and air replacement simulating start-up/shut-down cycles, was studied. The co-existence of H_2- and O_2-rich areas in the anode was clearly observed, which lasted a couple of times longer than the time predicted for the simple replacement of hydrogen and air. A serious corrosion was predicted at the cathode catalyst layer facing the remaining O_2-rich area. From the visualization, the shut-down process was indicated to be more serious because of the longer exposure of the inlet portion to O_2-rich atmosphere, compared to the outlet portion for the start-up process. After the deterioration of a cell performance with increasing the gas-exchange cycles, the time for replacement from hydrogen to air became shorter at the anode because of lowered oxygen consumption due to the suppressed supply of protons from the cathode to the anode near the inlet by the carbon corrosion. The replacement of air by hydrogen needed longer time as the cathode corrosion proceeded, and the mechanism of which was also discussed. The oxygen consumption for the current production was dominantly observed in the middle of the MEA because of the degradation of an MEA near the inlet and outlet of the cell. STEM images supported those results obtained by the visualization of oxygen consumption. Quantitative analyses of the cathode corrosion by visualizing carbon dioxide formed are now in progress.

Acknowledgment

This study was supported by the New Energy and Industrial Technology Development Organization (NEDO), Japan.

Appendix A. Supplementary data

Supplementary data associated with this article can be found, in the online version, at doi:10.1016/j.jpowsour.2010.11.092.

References

[1] C.A. Reiser, L. Bregoli, T.W. Patterson, J.S. Yi, J.D. Yang, M.L. Perry, T.D. Jarvi, Electrochem. Solid-State Lett. 8 (2005) A273–A276.
[2] H. Tang, Z. Qi, M. Ramani, J.F. Elter, J. Power Sources 158 (2006) 1306–1312.
[3] J.P. Meyers, R.M. Darling, J. Electrochem. Soc. 153 (2006) A1432–A1442.
[4] M. Cai, M.S. Ruthkosky, B. Merzougui, S. Swathirajan, M.P. Balogh, S.H. Oh, J. Power Sources 160 (2006) 977–986.
[5] Y. Shao, G. Yin, Y. Gao, J. Power Sources 171 (2007) 558–566.
[6] Z. Siroma, N. Fujiwara, T. Ioroi, S. Yamazaki, H. Senoh, K. Yasuda, K. Tanimoto, J. Power Sources 172 (2007) 155–162.
[7] X. Yu, S. Ye, J. Power Sources 172 (2007) 145–154.
[8] A.A. Franco, M. Gerard, ECS Meet. Abstr. 801 (2008) 1160–11160.
[9] A.A. Franco, M. Gerard, J. Electrochem. Soc. 155 (2008) B367–B384.
[10] S. Maass, F. Finsterwalder, G. Frank, R. Hartmann, C. Merten, J. Power Sources 176 (2008) 444–451.
[11] J. Wu, X.Z. Yuan, J.J. Martin, H. Wang, J. Zhang, J. Shen, S. Wu, W. Merida, J. Power Sources 184 (2008) 104–119.
[12] F. Ettingshausen, J. Kleemann, M. Michel, M. Quintus, H. Fuess, C. Roth, J. Power Sources 194 (2009) 899–907.
[13] J. Hu, P.C. Sui, S. Kumar, N. Djilali, Electrochim. Acta 54 (2009) 5583–5592.
[14] N. Yousfi-Steiner, P. Moçotéguy, D. Candusso, D. Hissel, J. Power Sources 194 (2009) 130–145.
[15] S. Zhang, X.-Z. Yuan, J.N.C. Hin, H. Wang, K.A. Friedrich, M. Schulze, J. Power Sources 194 (2009) 588–600.
[16] G. Maranzana, C. Moyne, J. Dillet, S. Didierjean, O. Lottin, J. Power Sources 195 (2010) 5990–5995.
[17] K. Tüber, D. Pócza, C. Hebling, J. Power Sources 124 (2003) 403–414.
[18] X.G. Yang, F.Y. Zhang, A.L. Lubawy, C.Y. Wang, Electrochem. Solid-State Lett. 7 (2004) A408–A411.
[19] K. Sugiura, M. Nakata, T. Yodo, Y. Nishiguchi, M. Yamauchi, Y. Itoh, J. Power Sources 145 (2005) 526–533.
[20] K. Sugiura, T. Shiramizu, T. Yamauchi, M. Yamauchi, S. Matsuzaki, N. Kada, Y. Itoh, ECS Trans. 12 (2008) 131–138.
[21] M.A. Hickner, N.P. Siegel, K.S. Chen, D.N. McBrayer, D.S. Hussey, D.L. Jacobson, M. Arif, J. Electrochem. Soc. 153 (2006) A902–A908.
[22] Y.-S. Chen, H. Peng, D.S. Hussey, D.L. Jacobson, D.T. Tran, T. Abdel-Baset, M. Biernacki, J. Power Sources 170 (2007) 376–386.
[23] A. Turhan, K. Heller, J.S. Brenizer, M.M. Mench, J. Power Sources 180 (2008) 773–783.
[24] A.Z. Weber, M.A. Hickner, Electrochim. Acta 53 (2008) 7668–7674.
[25] M.A. Hickner, N.P. Siegel, K.S. Chen, D.S. Hussey, D.L. Jacobson, M. Arif, J. Electrochem. Soc. 155 (2008) B294–B302.
[26] M.A. Hickner, N.P. Siegel, K.S. Chen, D.S. Hussey, D.L. Jacobson, M. Arif, J. Electrochem. Soc. 155 (2008) B427–B434.
[27] H. Murakawa, T. Ueda, T. Yoshida, K. Sugimoto, H. Asano, N. Takenaka, K. Mochiki, H. Iikura, R. Yasuda, M. Matsubayashi, Nucl. Instrum. Meth. A 605 (2009) 127–130.
[28] M.A. Hickner, N.P. Siegel, K.S. Chen, D.S. Hussey, D.L. Jacobson, J. Electrochem. Soc. 157 (2010) B32–B38.
[29] P.K. Sinha, P.P. Mukherjee, C.-Y. Wang, J. Mater. Chem. 17 (2007) 3089–3103.
[30] S.J. Lee, N.-Y. Lim, S. Kim, G.-G. Park, C.-S. Kim, J. Power Sources 185 (2008) 867–870.
[31] F.-Y. Zhang, S.G. Advani, A.K. Prasad, M.E. Boggs, S.P. Sullivan, T.P. Beebe Jr., Electrochim. Acta 54 (2009) 4025–4030.
[32] T. Sasabe, S. Tsushima, S. Hirai, K. Minami, K. Yada, ECS Trans. 25 (2009) 513–521.
[33] S. Tsushima, K. Teranishi, S. Hirai, Electrochem. Solid-State Lett. 7 (2004) A269–A272.
[34] S. Tsushima, T. Nanjo, S. Hirai, ECS Trans. 11 (2007) 435–443.
[35] K.W. Feindel, S.H. Bergens, R.E. Wasylishen, J. Power Sources 173 (2007) 86–95.
[36] J. Inukai, K. Miyatake, K. Takada, M. Watanabe, T. Hyakutake, H. Nishide, Y. Nagumo, M. Watanabe, M. Aoki, H. Takano, Angew. Chem. Int. Ed. 47 (2008) 2792–2795.
[37] J. Inukai, K. Miyatake, Y. Ishigami, M. Watanabe, T. Hyakutake, H. Nishide, Y. Nagumo, M. Watanabe, A. Tanaka, Chem. Commun. (2008) 1750–1752.